Articles

Synthesis of Ultrasensitive Magnetic Resonance Contrast Agents for Cancer Imaging Using PEG-Fatty Acid

Jaemoon Yang,[†] Tong-Il Lee,[‡] Jaemin Lee,[†] Eun-Kyung Lim,[†] Woochan Hyung,[†] Choong-Hwan Lee,[‡] Yong Jin Song,[§] Jin-Suck Suh,[||] Ho-Geun Yoon,[#] Yong-Min Huh,*[,||] and Seungjoo Haam*[,†]

Department of Chemical Engineering, College of Engineering, Yonsei University, Seoul 120-749, Republic of Korea, ATGen, Advanced Technology Research Center, 68 Yatap-dong, Bundang-gu, Seongnam-si, Gyeonggi-do, 463-816, South Korea, Department of Physics, College of Natural Science, Ajou University, Suwon 433-749, South Korea, Department of Radiology, College of Medicine, Yonsei University, Seoul 120-752, South Korea, and Department of Biochemistry and Molecular Biology, Center for Chronic Metabolic Disease Research, College of Medicine, Yonsei University, Seoul 120-752, South Korea

Received February 21, 2007. Revised Manuscript Received May 16, 2007

Diagnosis of cancer in the early stages requires sensitive magnetic resonance (MR) probes to detect low concentrations of magnetic substances. In this study, ultrasensitive magnetic resonance contrast agents (UMRCAs) composed of magnetic nanocrystals and amphiphilic block copolymers were synthesized for cancer detection using polyethylene glycol and fatty acid. The chemical structures and the compositions of PEGylated magnetic nanoparticles were analyzed. UMRCAs displayed remarkable colloidal stability and high sensitivity as MR probes. Furthermore, UMRCAs exhibited low cytotoxicity and excellent cancer detection ability in an in vivo animal model.

1. Introduction

Magnetic nanoparticles have received attention in several biomedical applications, including targeted drug delivery, cell labeling and separation, immunoassay, magnetic resonance imaging (MRI), and magnetic hyperthermia.[1−6] Of the available magnetic substances, magnetic nanocrystals synthesized by the thermal decomposition method are considered the most suitable material because of their high magnetic sensitivity and low toxicity.[5] In addition, magnetic sensitivity of magnetic nanocrystals could be enhanced with control of magnetic spin structure.[5c] However, due to their low colloidal stability in the aqueous phase, surface modifications are required to increase physicochemical stability. In general, magnetic nanoparticles in organic solvents are coated with inorganic/organic polymers or hydrophobic ligands that are exchanged with hydrophilic ligands for preparation of a stable aqueous magnetic solution.[7] PEGylation is one approach used to accomplish phase transfer to the aqueous phase.[8]

In this study, we report the synthesis of novel ultrasensitive magnetic resonance contrast agents (UMRCAs) composed of magnetic nanocrystals covered with amphiphilic block copolymers. The monodispersed $MnFe_2O_4$ nanocrystals were synthesized in organic solvent.[5c,9] $MnFe_2O_4$ presented excellent MR signal enhancement effects because of magnetic spinel structure under magnetic field. The magnetic susceptibility of $MnFe_2O_4$ was approximately magnetic spins of 5 μ_B, which was higher than that for other metal ferrites.[5c] To prepare stable UMRCAs using $MnFe_2O_4$ nanocrystals in the

* Corresponding author. Tel: 82-2-2123-2751 (S.H.); 82-2-2228-2375 (Y.-M.H.). Fax: 82-2-312-6401 (S.H.); 82-2-362-8647 (Y.-M.H.). E-mail: haam@yonsei.ac.kr (S.H.); ymhuh@yumc.yonsei.ac.kr (Y.-M.H.).

[†] Department of Chemical Engineering, Yonsei University.

[‡] ATGen, Advanced Technology Research Center.

[§] Ajou University.

[||] Department of Radiology, Yonsei University.

[#] Department of Biochemistry and Molecular Biology, Yonsei University.

(1) Yang, J.; Park, S. B.; Yoon, H. G.; Huh, Y.-M.; Haam, S. *Int. J. Pharm.* **2006**, *324*, 185.

(2) Song, H.-T.; Choi, J.-S.; Huh, Y.-M.; Kim, S.; Jun, Y.-W.; Suh, J.-S.; Cheon, J. *J. Am. Chem. Soc.* **2005**, *127*, 5732.

(3) Schneider, T.; Moore, L.; Jing, Y.; Haam, S.; Williams, P.; Fleischman, A.; Roy, S.; Chalmers, J.; Zborowski, M. *J. Biochem. Biophys. Methods* **2006**, *68*, 1.

(4) Kim, J.-I.; Wang, C.; Kuizon, S.; Xu, J.; Barengolts, D.; Gray, P.; Rubenstein, R. *J. Neuroimmunol.* **2005**, *158*, 112.

(5) (a) Jun, Y.; Huh, Y.-M.; Choi, J.; Lee, J.; Song, H.; Kim, S.; Yoon, S.; Kim, S.; Shin, J.; Suh, J.; Cheon, J. *J. Am. Chem. Soc.* **2005**, *127*, 5732. (b) Huh, Y.-M.; Jun, Y.; Song, H.; Kim, S.; Choi, J.; Lee, J.; Yoon, S.; Kim, K.; Shin, J.; Suh, J.; Cheon, J. *J. Am. Chem. Soc.* **2005**, *127*, 12387. (c) Lee, J.; Huh, Y.-M.; Jun, Y.; Seo, J.; Jang, J.; Song, H.; Kim, S.; Cho, E.; Yoon, H.; Suh, J.; Cheon, J. *Nat. Med.* **2007**, *13*, 95. (d) Li, Z.; Wei, L.; Gao, M.; Lei, H. *Adv. Mater.* **2005**, *17*, 1001.

(6) Park, S. I.; Hwang, Y. H.; Lim, J. H.; Kim, J. H.; Yun, H. I.; Kim, C. O. *J. Magn. Magn. Mater.* **2006**, *304*, 403.

(7) Michalet, X.; Pinaud, F. F.; Bentolila, L. A.; Tsay, J. M.; Doose, S.; Li, J. J.; Sundaresan, G.; Wu, A. M.; Gambhir, S. S.; Weiss, S. *Science* **2005**, *307*, 538. Gao, X.; Cui, X.; Levenson, R. M.; Chung. L. W. K.; Nie, S. *Nat. Biotechnol.* **2004**, *22*, 969.

(8) Graham, N. B. Poly(ethylene glycol) gels and drug delivery. In *Poly-(ethylene glycol) Chemistry*; Harris, J. M., Ed.; Plenum Press: New York, 1992.

(9) Sun, S.; Zeng, H.; Robinson, D. B.; Raoux, S.; Rice, P. M.; Wang, S. X.; Li, G. *J. Am. Chem. Soc.* **2004**, *126*, 273.

10.1021/cm070495s CCC: $37.00
Published on Web 07/17/2007

Scheme 1. Schematic Illustration of UMRCAs Synthesis

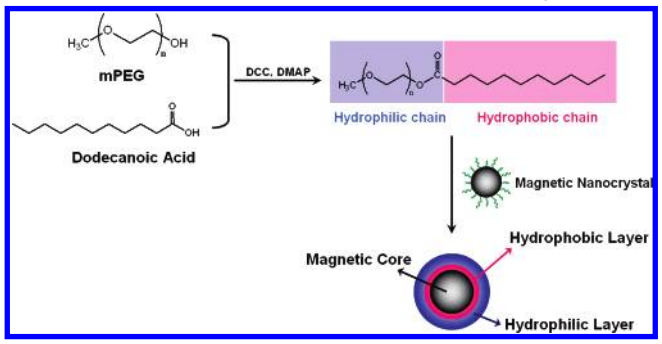

aqueous phase, we synthesized amphiphilic mPEG-DA block copolymers as stabilizers using the bioconjugation method. The morphology, size distribution, and composition of successful core−shell structures were analyzed. For application as MR probes, ultrasensitivity, colloidal stability, and biocompatibility of UMRCAs were evaluated. Furthermore, the ability of UMRCAs to detect cancer in vivo was investigated in animal models using MR imaging.

2. Experimental Section

2.1. Synthesis of Magnetic Nanocrystals. $MnFe_2O_4$ nanocrystals were synthesized by thermal decomposition.[5c] For the synthesis, 2 mmol iron (III) acetylacetonate, 1 mmol manganese (II) acetylacetonate, 10 mmol 1,2-hexadecanediol, 6 mmol dodecanoic acid, 6 mmol dodecylamine, and 20 mL of benzyl ether were mixed under a nitrogen atmosphere. The mixture was preheated to 150 °C for 30 min and then refluxed at 300 °C for 30 min. After being cooled to room temperature, the products were purified with an excess of pure ethanol. Approximately 10 nm magnetic nanocrystals were synthesized using the seed-mediated growth method.

2.2. Synthesis of mPEG-DA Amphiphilic Block Copolymers. For phase transference of $MnFe_2O_4$ nanocrystals to aqueous phase, mPEG-DA amphiphilic block copolymers were synthesized as stabilizers by the DCC method (Scheme 1).[10] An amount of 30 mmol dodecanoic acid (DA) and 10 mmol mPEG dissolved in 40 mL of anhydride methylene chloride was activated by adding 30 mmol of *N*,*N*′-dicyclohexylcarbodiimide (DCC) and 4-dimethylaminopyridine (DMAP). The reaction was carried out for 48 h at room temperature under a nitrogen atmosphere. The resulting products were filtered using a cellulose acetate syringe filter (pore size ≈ 200 nm) and dialyzed for two weeks against 10 mM sodium phosphate buffer (pH 7.4) using an MWCO 1000 dialysis tube. The products were filtered and stored under a vacuum for later use. The chemical structure of mPEG-DA was characterized by ^{1}H NMR (400 MHz, Varian INOVA400 NMR spectrometer) and FT-IR (Excalibur series). The critical micelle concentration of mPEG-DA was measured using conductivity.[11]

2.3. Synthesis of Ultrasensitive Magnetic Resonance Contrast Agents (UMRCAs). Thirty milligrams of $MnFe_2O_4$ nanocrystals was dissolved in 4 mL of hexane for the preparation of UMRCAs. This organic phase was added to 20 mL of sodium phosphate buffer containing 600 mg of mPEG-DA. After mutual saturation of the organic and continuous phase, the mixture was emulsified for 10 min with an ultrasonicator (ULH700S, Ulssohitech, Korea) at 300 W.[1] After solvent evaporation, the products were purified with three cycles of centrifugation at 20 000 rpm. The precipitated nanoparticles were redispersed in 4 mL of sodium phosphate buffer (10 mM, pH 7.4). The size distribution of the UMRCAs was analyzed by laser scattering (ELS-Z, Otsuka electronics). The saturation of magnetization was evaluated using a vibrating-sample magnetometer (Lakeshore, model 7300). The weight quantity of magnetic nanocrystals in the UMRCAs was analyzed with a thermogravimetric analyzer (SDT-Q600, TA instrument). X-ray diffraction measurements of $MnFe_2O_4$ nanocrystals were performed with a Rigaku D/max-RB (Tokyo, Japan) powder diffractometer and by image-plate photography using graphite-monochromatized Cu K radiation (l = 1.542 Å). Data were collected from 10 to 70° with a step size of 0.05° and step time of 5 s. The surface composition of the UMRCAs was evaluated by X-ray photoelectron

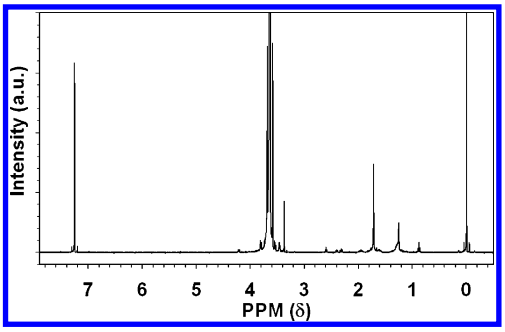

Figure 1. ^{1}H NMR spectra of mPEG-DA block copolymers.

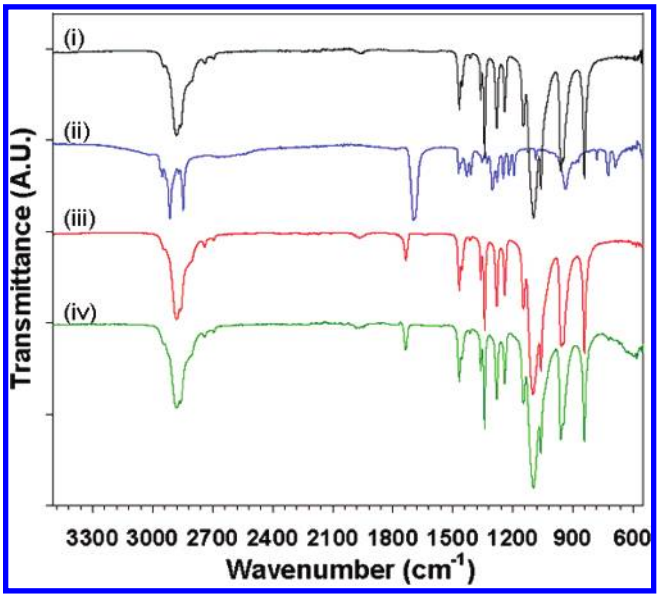

Figure 2. FT-IR spectra of mPEG (i), DA (ii), mPEG-DA block copolymers (iii), and UMRCAs (iv).

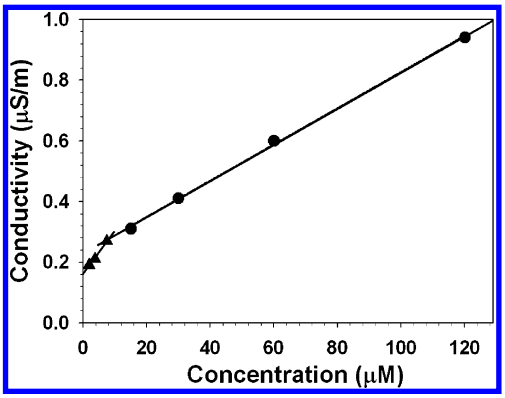

Figure 3. Determination of critical micelle concentration of mPEG-DA block copolymers using conductivity.

(10) Hermanson, G. T. *Bioconjugate Technique*; Academic Press: New York, 1996.
(11) Malmsten, M. *Surfactants and Polymers in Drug Delivery*; Marcel Dekker: New York, 2002.

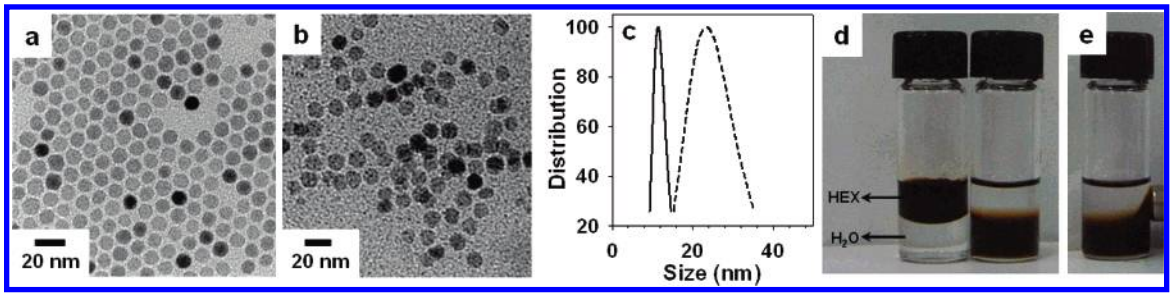

Figure 4. TEM images of (a) $MnFe_2O_4$ nanocrystals in hexane and (b) UMRCAs in aqueous solution. (c) Size distribution of $MnFe_2O_4$ nanocrystals and UMRCAs. (d) Solubility test against $MnFe_2O_4$ nanocrystals and UMRCAs. (e) Sensitive reaction of UMRCAs to the Nd−Fe−B magnet.

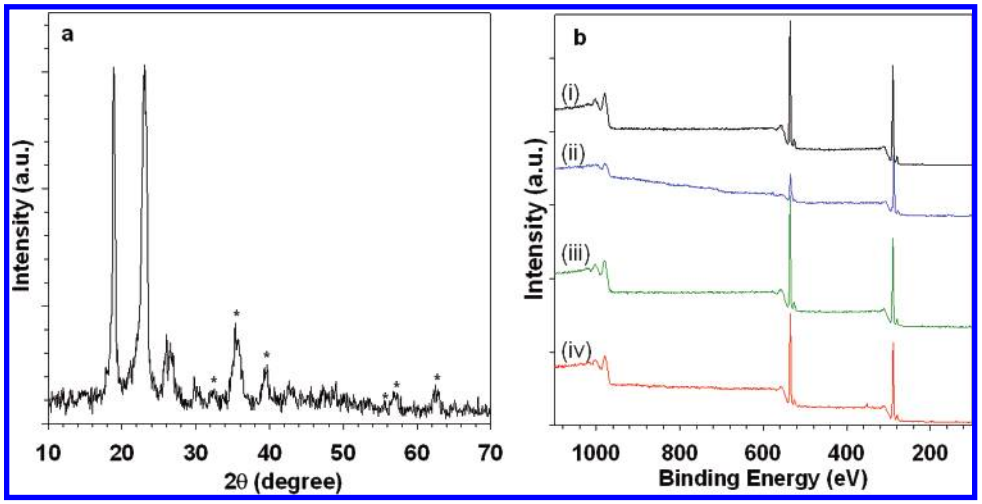

Figure 5. (a) XRD pattern of UMRCAs. The peaks of the $MnFe_2O_4$ nanocrystal structure are marked with asterisks (*). (b) XPS spectra of mPEG (i), DA (ii), mPEG-DA block copolymers (iii), and UMRCAs (iv).

spectroscopy (XPS, ESCALAB MK II, V.G. Scientific Ltd.). Inductively coupled plasma mass spectroscopy (ICP−MS) was used for compositional analysis of UMRCAs. ICP−MS analysis was carried out on a Perkin-Elmer Sciex Elan 6100 instrument (Wellesley, MA) using an argon plasma flame and dual detector mode.

2.4. Evaluation of Colloidal Stability of UMRCAs. The colloidal stability of the prepared UMRCAs was determined from their resistance to sodium chloride and pH-induced nanoparticle aggregation. A 100 μL nanoparticle suspension (20 mg/mL) was added to 5 mL of sodium chloride solutions of varying concentration and pH (0−1.0 M of sodium chloride and pH 5−10) at 37 °C. After 24 h, the size of the suspension was measured using laser scattering.

2.5. Determination of Cell Viability by MTT Assay. NIH3T6.7 cells (ATCC, Manassas, VA) were maintained in DMEM (Gibco, NY), containing 10% (v/v) fetal bovine serum, 100 U/mL penicillin and 0.1 mg/mL streptomycin in a 5% CO_2 humidified atmosphere at 37 °C. Cytotoxicity of UMRCAs was evaluated by measuring the inhibition of cell growth using the MTT assay. Briefly, cells were plated at a density of 4×10^3 cells/mL in 96-well plates and treated with UMRCAs at concentrations from 1×10^{-4} to 10 mg/mL for 72 h. Cell viabilities were obtained by calculating the ratio of the number of viable cells in the treated culture compared with nontreated control cells.

2.6. MR Imaging Procedure. All MR imaging experiments were performed with a 1.5 T clinical MRI instrument with a micro-47 surface coil (Intera; Philips Medical Systems, Best, The Netherlands). R2 relaxivities of UMRCAs were measured at room temperature by the Carr−Purcell−Meiboom−Gill (CPMG) sequence: TR = 10 s, 32 echoes with 12 ms even echo space, number of acquisitions = 1, point resolution of 156 × 156 μm^2, section thickness of 0.6 mm. R2 was defined as 1/T2 with units of s^{-1}. For T2-weighted MR imaging of a live mouse, the following parameters were adopted: resolution of 234 × 234 μm^2, section thickness of 2.0 mm, TE = 60 ms, TR = 4000 ms, number of acquisitions = 1. For T2 mapping of a live mouse, the following parameters were adopted: point resolution of 234 × 234 μm^2, section thickness of 2.0 mm, TE = 20, 40, 60, 80, 100, 120, 140, 160 ms, TR = 4000 ms, number of acquisitions = 2.

3. Results and Discussion

The process for preparation of stable inorganic/organic hybrids in the aqueous phase is schematically illustrated in Scheme 1. The process involves two steps: (i) synthesis of amphiphilic block copolymers, and (ii) assembling the magnetic nanoparticles by nanoemulsion methods. First, the amphiphilic block copolymers were synthesized using hydrophilic mPEG and hydrophobic DA by the DCC method. The carboxyl group of DA was activated by DCC and DMAP, and the activated functional group was then attacked by the hydroxyl group of mPEG as a nucleophile. The amphiphilic mPEG-DA was characterized using ^1H NMR (400 MHz, $CDCl_3$) by δ values of 3.64 ($-(OCH_2CH_2)_n-$ of PEG backbone), 1.72, 1.25 ($-(CH_2)_{10}-$ of DA chain), 0.88 ($-CH_3$ of DA chain) (Figure 1). Furthermore, using FT-IR spectra, we confirmed that the carboxyl group of DA (1695 cm^{-1}) was converted into an ester group (1734 cm^{-1}) of mPEG-DA after conjugation with the hydroxy group of

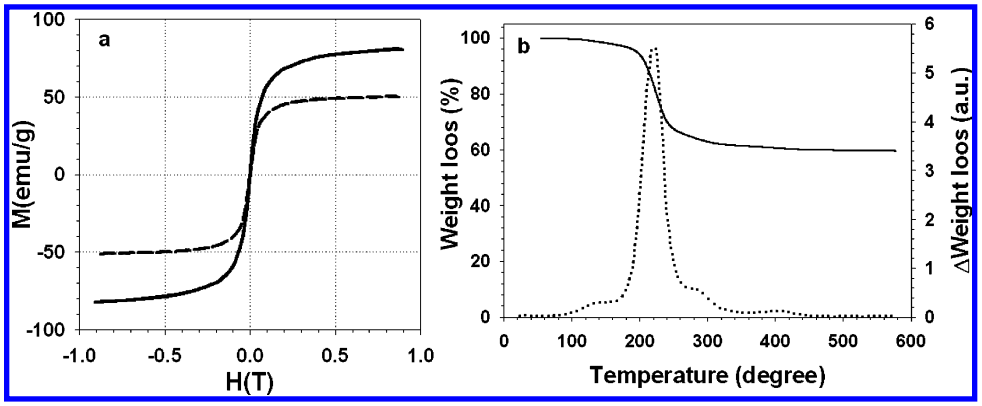

Figure 6. (a) Magnetic hysteresis loops of magnetic nanocrystals (black solid line) and UMRCAs (gray dashed line). (b) Thermogravity analysis of UMRCAs; weight loss vs temperature (black solid line), Δweight loss vs temperature (gray dotted line).

mPEG (Figure 2). These results demonstrated that the amphiphilic block copolymers were synthesized easily and successfully by bioconjugation chemistry.

To evaluate the potential as a surfactant, the critical micelle concentration (CMC) of amphiphilic mPEG-DA was measured using conductivity. When the micelles were formed, the slope of conductivity against the concentration of block copolymers decreased because the micelles inhibited the transfer of ions in the aqueous phase; the slope was 0.015μS m^{-1} μM^{-1} before micelle formation compared with 0.006 μS m^{-1} μM^{-1} after micelle formation. Although the hydrophobic chain of DA was shorter than the hydrophilic chain of mPEG, the CMC of mPEG-DA was relatively low at 9.91 μM (Figure 3).

Uniform $MnFe_2O_4$ nanocrystals (~12 nm) were synthesized at high temperature by a thermal decomposition process. The morphology of $MnFe_2O_4$ nanocrystals revealed by transmission electron microscopy (TEM) is shown in Figure 4a. These magnetic nanocrystals synthesized in the organic solvents are not soluble in the aqueous phase without surface modifications.[7] To increase the solubility and colloidal stability in aqueous phase, we introduced mPEG-DA to cover the magnetic nanocrystals. Because of the hydrophobic interaction of magnetic nanocrystals with the DA component of amphiphilic block copolymers, the PEG-coated magnetic nanoparticles (UMRCAs) were built up by a nanoemulsion method. UMRCAs were well-dispersed in the aqueous phase (Figure 4b), and the size of the UMRCAs determined using laser scattering was 22.3 ± 6.5 nm, slightly larger than the magnetic nanocrystals because of the PEG molecules on the surface of UMRCAs (Figure 4c). The amphiphilic block copolymers effectively encapsulated magnetic nanocrystals, while simultaneously increasing water solubility. Thus, these PEGylated UMRCAs could be dissolved in aqueous phase (Figure 4d). In addition, when a Nd−Fe−B magnet (0.35 T) was applied to the wall of the vial, the UMRCAs showed a sensitive reaction toward the magnet (Figure 4e).

The presence and crystallinity of magnetic substances in the UMRCAs was verified using FT-IR and XRD. In FT-IR spectra, a characteristic peak was demonstrated at 580 cm^{-1} in the UMRCAs containing the $MnFe_2O_4$ nanocrystal that

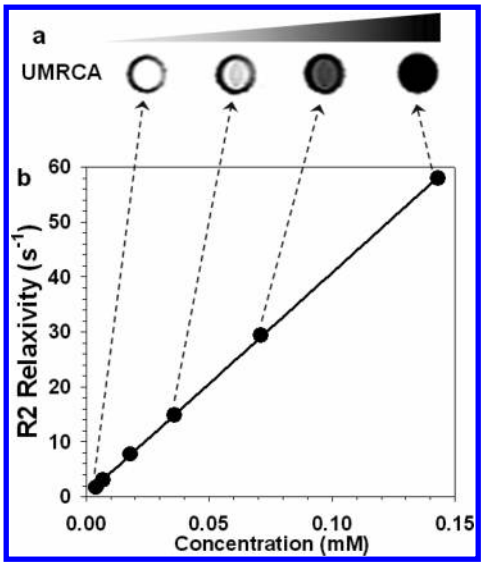

Figure 7. (a) T2-weighted MR images of UMRCAs in aqueous solution. (b) Graph of R2 relaxivity against the concentration of UMRCAs.

was due to the presence of the Fe−O bond (Figure 2d).[12] In addition, the ester group of mPEG-DA was also confirmed at 1735 cm^{-1}. The X-ray diffraction pattern of UMRCAs is shown in Figure 5a. Although $MnFe_2O_4$ nanocrystals were covered with mPEG-DA block copolymers, the spinel structure of $MnFe_2O_4$ nanocrystals could be confirmed in the XRD patterns (asterisk in Figure 5a).[5c] The chemical composition of the UMRCAs surface was analyzed using XPS spectra. The Fe 2p peaks of $MnFe_2O_4$ in the UMRCAs were too small to identify at 700−740 eV, whereas the carbon/oxygen ratio of the UMRCAs surface was similar in composition to that of mPEG-DA (Figure 6). These results demonstrated that the UMRCAs were assembled with a well-tailored core shell structure.

To assess the potential of UMRCAs in MR probe applications, we investigated sensitivity to a magnetic field. The hysteresis loops of $MnFe_2O_4$ nanocrystals and UMRCAs were investigated using a VSM at 300 K (Figure 6a). The prepared UMRCAs exhibited superparamagnetic behavior without magnetic hysteresis. The saturation of magnetization of $MnFe_2O_4$ nanocrystals and UMRCAs at 900 mT was 80.8 emu/g and 47.0 emu/g, respectively. Because of the presence

(12) Rocchiccioli-Deltcheff, C.; Franck, R.; Cabuil, V.; Massart, R. *J. Chem. Res.* **1987**, 127.

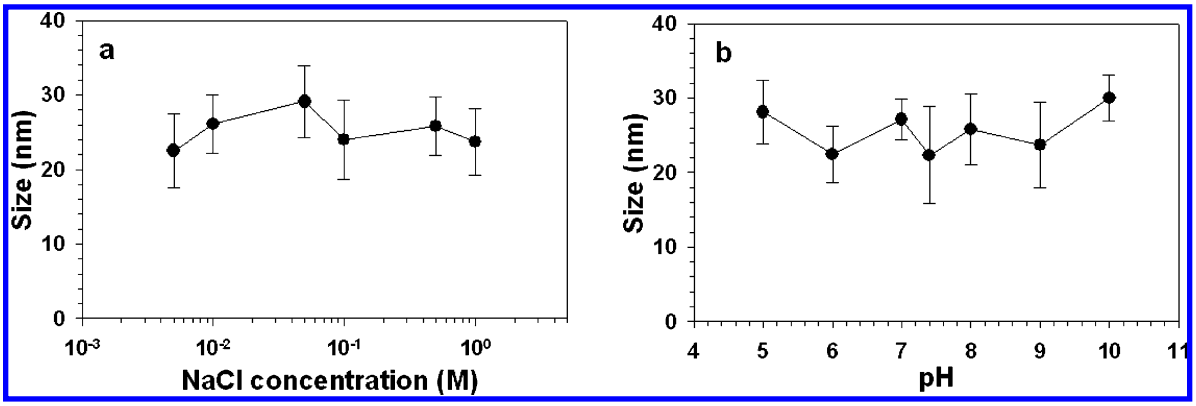

Figure 8. Size of UMRCAs plotted against NaCl concentration and pH conditions.

of organic components, the saturation of magnetization of UMRCAs was relatively lower than that of $MnFe_2O_4$ nanocrystals. The actual amount of magnetic nanocrystals in the UMRCAs was determined by TGA to be 59.6% w/w (Figure 6b). The Fe and Mn elemental-based saturation of magnetization of UMRCAs was similar to that of pure magnetic nanocrystals.

We next investigated the induced MR signals and magnetic properties of the UMRCAs to evaluate their diagnostic capability. The spin−spin relaxation time (T2) weighted spin−echo MR images of UMRCAs increased significantly with increasing concentration of Fe + Mn (Figure 7a). Similarly, the relaxivity (R2) of UMRCAs linearly increased under these conditions. The relaxivity coefficient of UMRCAs by magnetic field was 404 mM^{-1} s^{-1}, which was almost 2.5 times higher than the values of other recent reports.[13,14]

Colloidal stability of aqueous UMRCAs is an essential requirement for use as a MR probe. We therefore measured UMRCAs size in various salt concentrations and over a wide range of pH using laser scattering. The colloidal stabilities of UMRCAs in aqueous solution are plotted against the concentration of sodium chloride and pH in Figure 8. The size of UMRCAs did not change over these condition ranges because PEG chains on the surface of UMRCAs prevented the aggregation of nanoparticles.[8] Furthermore, there were no precipitates after centrifugation of the UMRCAs at 21 000 for 1 h.

To evaluate the biocompatibility of UMRCAs as a MR contrast agent, we investigated the cytotoxicity of UMRCAs using the MTT assay. UMRCAs exhibited low cytotoxicity toward NIH3T6.7 cells at high concentrations (1 mg/mL) (Figure 9). Importantly, although the cells were incubated with the PEGylated UMRCAs for a long time (72 h), high levels of cell viability were observed, indicating low overall cytotoxicity.

We next performed MR imaging of an in vivo mouse model using well-dispersed aqueous UMRCAs as an MR contrast agent for passive cancer detection. Nude mice were implanted in the proximal thigh with NIH3T6.7 cells. MR imaging of mice carrying tumors ~8 cm^3 in volume was performed at different time points after intravenous tail

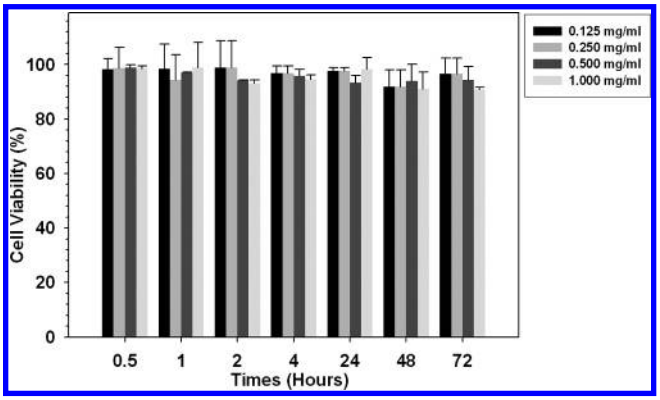

Figure 9. Cell viability of NIH3T6.7 cells treated with various concentrations of UMRCAs measured by the MTT assay.

injection of 80 μg Fe + Mn UMRCAs (preinjection and immediately, 1, 2, and 5 h postinjection) (Figure 10). The injection value was low, approximately 30% that of previous works.[5b,15] The growth of tumor cells was more rapid than normal cells. Thus, neoangiogenic vessels of tumor tissue were more generated to supply the oxygen and nutritive elements. The tumor has a change by the balance between its rapid growth and its vascular supply so that minimal vascular supplying parts should be fallen into necrosis or apoptosis of that tumor.[16,17] These parts show high signal intensity in T2-weighted MR images because of increase of water content.[18] In the end, the tumor tissue demonstrated heterogeneous bright color rather than the normal tissue on T2-weighted images (Figure 10a). After injection of the UMRCAs, however, the T2 value was immediately decreased at the tumor site along intratumoral blood vessels, and a continuous increase in $\Delta R2/R2_{Pre}$ value was observed (26.4% after injection, ~40.3% at 1 h, ~44.1% at 2 h, and ~45.8% at 5 h) because the nanoparticles were diffused and permeated to tumor tissues across corresponding vascular distributions due to EPR effect.[19] In Figure 10f−j, we also could confirm the remarkable change of R2 values against tumor site by UMRCAs. At preinjection state, blue and green colors were dominant (Figure 10f). After injection of UMRCAs into the

(13) Hu, F.; Wei, L.; Zhou, Z.; Ran, Y.; Li, Z.; Gao, M. *Adv. Mater.* **2006**, *18*, 2553.
(14) Berret, J.; Schonbeck, N.; Gazeau, F.; Kharrat, D.; Sandre, O.; Vacher, A.; Airiau, M. *J. Am. Chem. Soc.* **2006**, *128*, 1755.
(15) Li, Z.; Wei, L.; Gao, M.; Lei, H. *Adv. Mater.* **2005**, *17*, 1001.
(16) Cuenod, C. A.; Fournier, L.; Balvay, D.; Guinebretière, J.-M. *Abdominal Imaging* **2006**, *31* (2), 188.
(17) Sengupta, S.; Eavarone, D.; Capila, I.; Zhao, G.; Watson, N.; Kiziltepe, T.; Sasisekharan, R. *Nature* **2005**, *28*, 568.
(18) Hanahan, D.; Weinberg, R. A. *Cell* **2000**, *100*, 57.
(19) Gao, X.; Cui, Y.; Levenson, R. M.; Chung, L. W.; Nie, S. *Nature Biotechnol.* **2004**, *22*, 969.

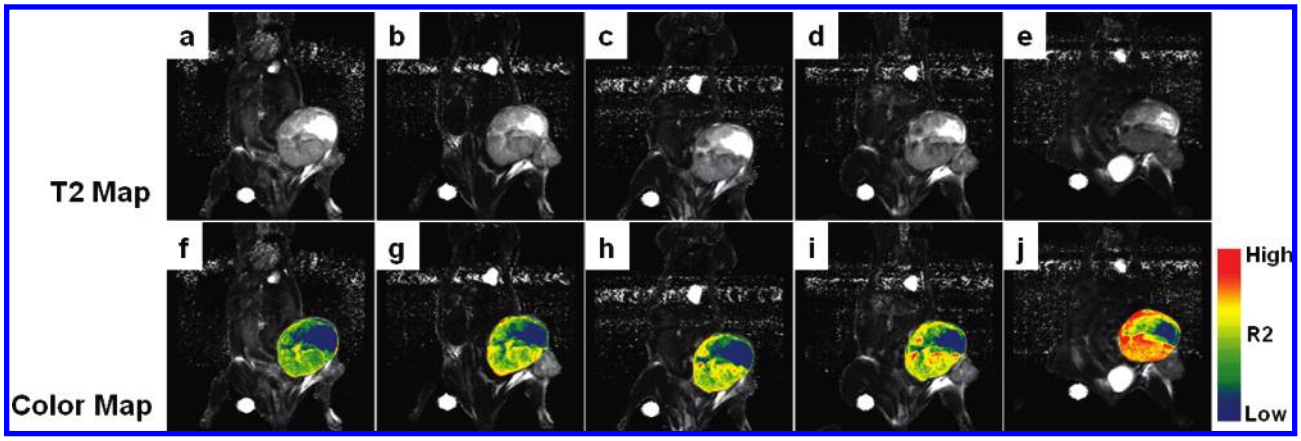

Figure 10. MR images of nude mice implanted with NIH3T6.7 cells at proximal thigh region of mouse model after injection of the UMRCAs and their color maps: (a, f) preinjection, and (b, g) immediately, (c, h) 1 h, (d, i) 2 h, and (e, j) 5 h after injection of UMRCAs.

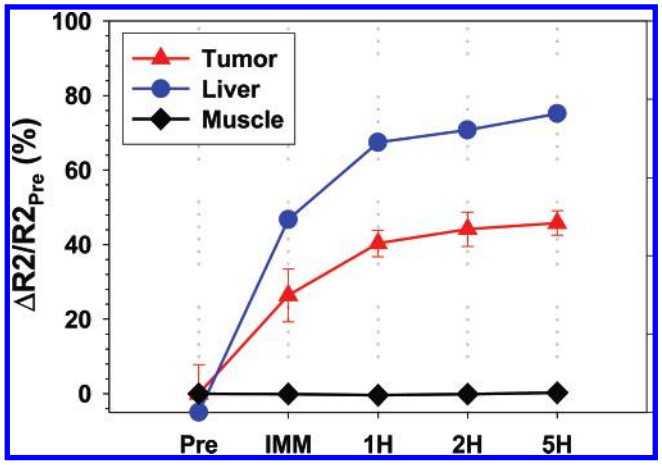

Figure 11. $\Delta R2/R2_{Pre}$ plot at tumor, liver, and muscle site against time before and after injection of UMRCAs.

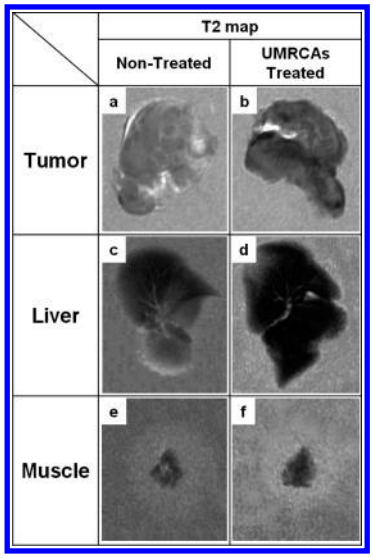

Figure 12. Ex vivo MR images of (a, b) tumor tissue, (c, d) liver, and (e, f) muscle of mouse model: the UMRCAs nontreated tumor (a, c, e) and UMRCAs treated tumor tissue (b, d, f).

mouse model, however, the red color gradually spread out, following the peripheral blood vessel and central vessel of tumor area.[18,20] The images were gradually altered with red color and yellow colors as time went by. The red color means a higher R2 (lower T2) value than blue color and other colors. The UMRCAs were coated with poly(ethylene glycol) (PEG) and their sizes were small, ~22 nm. Thus, these PEGylated nanoparticles could avoid uptake due to RES (reticuloendothelial system) by liver or spleen, so that these nanoparticles have a greater chance to detect the tumor region (Figure 11).[21,22] As shown in Figure 11, normal tissues (muscle) demonstrated a minimal change in $\Delta R2/R2_{Pre}$ values in comparison with the tumor site. In addition, we conducted the ex vivo MR imaging from the in vivo mouse model after injection of UMRCAs (Figure 12). In ex vivo MR imaging, the blood eliminated tumor tissue by formalin perfusion presented partially black color.[23] This heterogeneous enhancement of MR intensity comes from blood pool effect or enhanced permeation and retention effect of MRCAs.[24,25] Injected UMRCAs circulated in the blood vessel of mouse model and were delivered to the tumor site. In addition, PEGylated UMRCAs remained in the blood pool for a longer period of time as compared to the nonPEGylated nanoparticles.[26] Thus, the change of MR images could be confirmed as follow blood vessels. On the other hand, nontreated tumor tissue did not present a color change. Furthermore, normal muscle did not significantly change and the $\Delta R2/R2_{Non-treated}$ value of the tumor tissue was 145.7 times larger than that of normal muscle because the UMRCAs could not permeate into the normal tissue (Figure 13). Therefore, the UMRCAs as passive targeting agents could avoid a phagocyte by the RES and act for cancer detection successfully. The PEGylated UMRCAs in the blood can play a role in diagnosis of the tumor site for a long time.[27] The nude mice lived for more than a month after the experiment, confirming the biocompatibility of UMRCAs in this animal model. These results imply that it is possible to use UMRCAs as an MR probe to reach and detect cancer of the proximal thigh region.

(20) Huwart, L.; Michoux, N.; Van Beers, B. E. *J. Radiol.* **2007**, *88*, 331.
(21) Roberts, M. J.; Bentley, M. D.; Harris, J. M. *Adv. Drug Delivery Rev.* **2002**, *54* (4), 459.
(22) Ichikawa, K.; Hikita, T.; Maeda, N.; Takeuchi, Y.; Namba, Y.; Oku, N. *Biol. Pharm. Bull.* **2004**, *27*, 433.
(23) Gabriel, H. A.; Feng, C.; Mendelson, E. B.; Benjamin, S. *Am. J. Roentgenol.* **2004**, *182*, 1081.
(24) Nolte-Ernsting, C.; Adam, G.; Bucker, A.; Berges, S.; Bjornerud, A.; Gunther, R. W. *Am. J. Roentgenol.* **1998**, *171*, 107.
(25) Allkemper, T.; Bremer, C.; Matuszewski, L.; Ebert, W.; Reimer, P. *Radiology* **2002**, *223*, 432.
(26) Kaul, G.; Amiji, M. *J. Drug Targeting* **2004**, *12* (9−10), 585.
(27) Tanaka, T.; Shiramoto, S.; Miyashita, M.; Fujishima, Y.; Kaneo, Y. *Int. J. Pharm.* **2004**, *277*, 39.

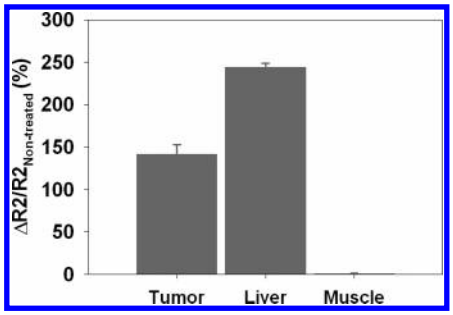

Figure 13. Biodistribution of the UMRCAs in vivo model: $\Delta R2/R2_{nontreated}$ plot against ex vivo MR images of tumor tissue, liver, and muscle of mouse model.

4. Conclusion

These studies describe the development of ultrasensitive magnetic resonance contrast agents (UMRCAs) composed of magnetic nanocrystals and amphiphilic mPEG-DA block copolymers. PEGylation of organic magnetic nanocrystals increased solubility in the aqueous phase. High biocompatibility of UMRCAs was demonstrated in a mouse model. Furthermore, cancer detection in an animal model using UMRCAs and MR imaging demonstrated that UMRCAs have excellent sensitivity and feasibility as MR contrast agents. Such agents represent a novel strategy with potential applications in various biomedical fields including diagnosis of cancer, drug delivery, and cell separation.

Acknowledgment. This work was supported by KOSEF through the National Core Research Center for Nanomedical Technology (R15-2004-024-00000-0 and R01-2006-000-10023-0), the National R&D Program for Cancer Control, Ministry of Health & Welfare, Republic of Korea (0620190-1), and the Yonsei University Research Fund of 2006.

CM070495S